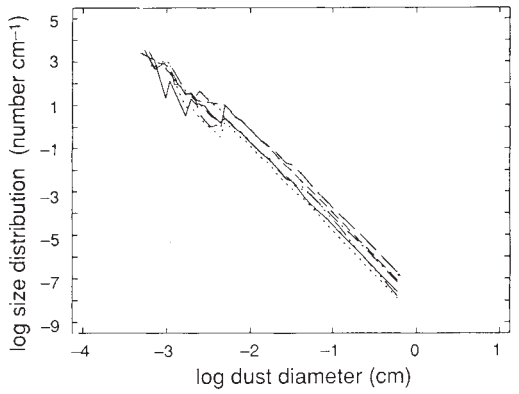

FIG. 3 Time-averaged and normalized size distribution for a dust bulk density of 1 g cm^{-3} (the diameters depend inversely on the assumed density). See Table 1 for line styles. The power index of the distribution of P/Schwassmann-Wachmann 1 is −3.3±0.3.

The results are plotted in Fig. 2, and in Fig. 1 the corresponding fits of the observed tail are reconstructed by means of the solution F. The index $u = -\frac{1}{2}$ gives velocities and loss rates decreasing in time; these are unrealistic results which should be rejected because the comet approaches the Sun. The instabilities of the loss rate for $t > -200$ may be an artefact due to the inversion of the ill-posed problem[20]. If the size distribution has a power index larger than −4, the dust mass is independent of the lower limit of the sizes but strongly dependent on the upper one. The ejection of grains much larger than 2 cm at 6 AU from the Sun is, however, improbable. The most reliable error estimate of the mass loss rate is given by the dispersion of the results for different combinations of the free parameters u and w (ref. 20).

Our results give a mass loss rate of $(6 \pm 3) \times 10^5$ g s^{-1}. Because all the grains are injected in bound orbits, the same rate of change of mass goes to replenish the interplanetary dust cloud. This contribution alone balances 6±3% of the required mass in the interplanetary cloud[2]. The rate of loss may be too large to be explained by water-ice sublimation[12]; phase transitions between water-ice states[21] may account for the outbursts which probably eject much smaller particles[22] and therefore lower dust masses. The different conditions of dust ejection and the uncertainties in models of gas drag on very large grains[23] do not allow conclusive comparisons between our velocities and the lower ones derived from analysis of the P/Tempel 2 trail[14]. Extended observations[12] combined with our mass loss rate, explain the persistent coma as the result of steady activity in SW1 rather than of overlaps of outburst shells[24].

The high mass-loss rate is consistent with the power index of the time-averaged size distribution (−3.3±0.3, Fig. 3). This power index is higher than the value obtained for comets P/Encke and P/D'Arrest[17], and is close to the index of the dust released by the new comet Wilson 1987VII well before perihelion[25] ('new' in the sense that it has recently entered the Solar System from the Oort cloud). Because the dust of P/Encke and P/D'Arrest was released within the orbit of Mars, such differences suggest that the size distribution of comet dust depends on its distance from the Sun when it is produced, not only on the comet's age. A dust production process different from the usual one (which is based on a water-dominated coma[26]) is therefore plausible and compatible with the large mass loss rate and the observation of a CO^+ tail[8]. The results suggest a coma dominated by CO or CO_2 beyond Mars. □

Received 9 December 1991; accepted 14 July 1992.

1. Maurette, M., Jehanno, C., Robin, E. & Hammer, C. *Nature* **328,** 699–702 (1987).
2. Grün, E., Zook, H. A., Fechtig, H. & Giese, R. H. *Icarus* **62,** 244–272 (1985)
3. Whipple, F. L. in *Zodiacal Light and the Interplanetary Medium* (ed. Weinberg, J.) NASA SP-150, 409–426 (1967).
4. Newburn, R. L. & Spinrad, H. *Astr. J.* **90,** 2591–2608 (1985).
5. Newburn, R. L. & Spinrad, H. *Astr. J.* **97,** 552–565 (1989).
6. Sykes, M. V. in *Origin and Evolution of Interplanetary Dust* (Reidel, Dordrecht, in the press).
7. Fulle, M. *Astr. Astrophys.* **217,** 283–297 (1989).
8. Jockers, K., Bonev, T., Ivanova, V. & Rauer, H. *Astr. Astrophys.* **260,** 455–464 (1992).
9. Hanner, M. S. & Newburn, R. L. *Astr. J.* **97,** 254–261 (1989).
10. Rickman, H. in *Dynamics of Comets: Their Origin and Evolution* (ed Carusi, A. & Valsecchi, G. B.) 149–172 (Reidel, Dordrecht, 1985).
11. Froeschle, C., Klinger, J. & Rickman, H. in *Asteroids, Comets, Meteors* (eds Lagerkivst, C. & Rickman, H.) 215–224 (Uppsala Univ. Press, Uppsala, 1983).
12. Jewitt, D. *Astrophys. J.* **351,** 277–286 (1990).
13. Delsemme, A. H. in *Diversity and Similarity of Comets* ESA SP-278, 19–30 (1987).
14. Sykes, M. V., Lien, D. J. & Walker, R. G. *Icarus* **86,** 236–247 (1990).
15. McDonnell, J. A. M. Lamy, P. L. & Pankiewicz, G. S. in *Comets in the Post-Halley Era* (eds Newburn, R.L.Jr, Neugebauer, M. Rahe, J.) 1043–1074 (Kluwer, Dordrecht, 1991).
16. Finson, M. L. & Probstein, R. F. *Astrophys. J.* **154,** 327–352 (1968).
17. Fulle, M. *Astr. Astrophys.* **230,** 220–226 (1990).
18. Marquardt, D. W. *Technometrics* **12,** 591–602 (1970).
19. Burns, J. A., Lamy, P. L. & Soter, S. *Icarus* **40,** 1–48 (1979).
20. Fulle, M., Cremonese, G., Jockers, K. & Rauer, H. *Astr. Astrophys.* **253,** 615–624 (1992).
21. Smoluchowski, R. in *Ices in the Solar System* (eds Klinger, J., Benest, D., Dollfus, A. & Smoluchowski, R.) 397–406 (Reidel, Dordrecht, 1985).
22. Cochran, A. L., Cochran, W. D. & Barker, E. S. *Astrophys. J.* **254,** 816–822 (1982).
23. Crifo, J. F. in *Comets in the Post-Halley Era* (eds Newburn, R. L. Jr, Neugebauer, M. & Rahe, J.) 937–990 (Kluwer, Dordrecht, 1991).
24. Sekanina, Z. *Astr. J.* **100,** 1293–1314 (1990).
25. Cremonese, G. & Fulle, M. *Astr. J.* **100,** 1285–1292 (1990).
26. Delsemme, A. H. in *Comets* (ed. Wilkening, L. L.) 85–130 (Univ. of Arizona Press, Tucson, 1982).

Coalescence reactions of fullerenes

Chahan Yeretzian*, Klavs Hansen*†, François Diederich‡ & Robert L. Whetten*

* Department of Chemistry and Biochemistry, University of California, Los Angeles, California 90024-1569, USA
† Niels Bohr Institute, 4000 Roskilde, Denmark
‡ Laboratorium für Organische Chemie, ETH-Zentrum, Universitätsstrasse 16, CH-8092 Zürich, Switzerland

THE production of fullerene molecules typically involves extreme high-temperature conditions (electric arcs[1], flames[2] or resistive heating[3]), and the reactive processes involved are poorly understood. Once separated[4,5], these molecules can undergo several important reactions, including formation of charge-transfer[6,7] and adduct[8,9] compounds, and the encapsulation of atoms[10–12]. Here we present evidence for coalescence reactions between fullerene molecules: mass spectrometric measurements on hot, dense vapours of small fullerenes (C_{60} and C_{70}) reveal the formation of stable higher fullerenes which are multiples of the initial masses. The heat of coalescence is released through emission of small, even-numbered fragments which, in a very dense vapour, are efficiently captured by other coalesced fullerenes. These findings have implications for the mechanisms of fullerene formation and growth, and may open the way to new synthetic routes to selected higher fullerenes and encapsulation compounds.

The fullerenes are a series of highly cohesive all-carbon molecules, C_{2p+20}, whose structures are closed bonding nets consisting of 12 pentagonal and p hexagonal rings[13,14]. Giant fullerenes, with very large p, may therefore have properties tending toward those of a single, closed graphitic sheet: an infinite, or periodic, extension of six-membered rings. For the molecule C_{60}, the cohesive energy per atom is already only 0.4 eV per atom below (less stable than) graphite, recovering 95% of the bulk binding[15,16]. First-principles and semi-empirical calculations[17–19] indicate that the cohesion per atom increases steadily with p, from C_{60} to C_{70} and towards C_{96}; a particularly stable form of C_{120} is estimated to be 0.16 eV per atom, or nearly 20 eV, more stable than two C_{60} molecules[17,18]. This increase in cohesive energy per atom provides a strong driving force for fullerene coalescence: reactions in which two small fullerenes merge and open up to form a larger net or giant fullerene. Given the clear existence of this thermodynamic driving force, the only question is one of the kinetics of the growth at realistic temperatures and densities.

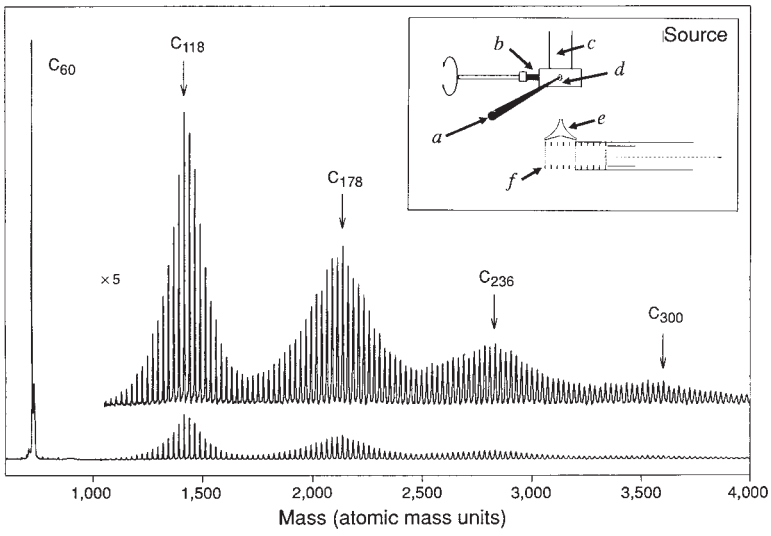

FIG. 1 Distribution of carbon clusters produced by high-intensity irradiation of pure C_{60} powder under a helium flow (detecting positively charged clusters). All the higher peaks are even-numbered. To the far left is the solitary C_{60} peak. The maxima indicated are near-multiples of the C_{60} starting material, that is, near C_{60p} where $p=2$, 3, 4, 5. Note the nearly complete absence of the fragments $n=58$ and 56, and also the next higher special fullerenes, $n=70$, 84 and so on. Inset, detail of the source. To generate the spectrum shown, a slightly focused ultraviolet laser pulse *a* (Nd:YAG, 266 nm, 6 ns) at a fluence near 2 mJ cm^{-2} (at least three times as high as used in conventional compositional analysis[4]), is fired at the sample *b* simultaneously with a 10-bar helium flow from a pulsed gas valve *c*. Desorbed molecules, both charged (positive and negative) and neutral, are swept along by the helium jet through a flow channel *d*, 2 mm long by 4 mm wide and a skimmer *e*, and into the pulsed extraction region *f* of a reflectron time-of-flight spectrometer. Charged clusters are extracted perpendicular to the helium flow by an electric-field pulse, so that the charged component of the vapour is detected without further exposure to ionizing radiation.

We have observed these processes using the following experimental approach (Fig. 1). A pulse of hot, dense vapour is generated by laser desorption of a fullerene film into an inert gas flowing at near-sonic speed. After a short time ($<10^{-3}$ s), the gas expands into vacuum, terminating molecular collisions, and the composition of the gas mixture is measured by mass spectrometry (for details, see Fig. 1). Mass spectra are signal-averaged over many such pulses, and it has been verified that the purified fullerene film is not transformed by this treatment. Substantial quantities of material are consumed, of the order of 1 mg per hour.

Under ordinary low-yield conditions (low fluence, small irradiated spot size or no carrier gas), the desorbed vapour consists entirely of the monomeric species present in the solid, with essentially no fragmentation[4]. Desorption with a tightly focused laser gives the monomer and its fragments. Use of large-area irradiation at higher total intensities can yield mass distributions showing negligible fragmentation to smaller fullerenes, but with a very broad, nearly smooth distribution of C_{2n} species extending from C_{70} to C_{400} or higher (not shown), which is not readily distinguished from those produced by, for example condensation of laser-generated graphite vapour[13].

Through careful control of the vapour density and heating, achieved by varying the laser fluence and irradiated spot size, we can obtain very different distributions of giant carbon molecules (Figs 1 and 2). For C_{60} vapour in Fig. 1, the distribution varies smoothly, but has strong oscillations with peaks near multiples of C_{60}: near C_{120}, C_{180}, C_{240} and C_{300}. Figure 2*a* shows a similar pattern at slightly higher fluences, where a greater fraction of the C_{60} is converted to higher masses. This pattern indicates the aggregation of individual molecules into giant aggregates, $mC_{60} \rightarrow C_{60m}$, although other processes are clearly involved.

To clarify the processes leading to distributions such as those in Figs 1 and 2*a*, the extent of reaction must be much more restricted. We did this by decreasing the fluence and increasing the sensitivity to the few high-mass species formed (Figs 2*b*, 2*c* and 3). The mass distribution about each maximum become asymmetric, with step-like decreases displaced from the simple combination product by a single C_2 unit: twice C_{60} yields predominantly C_{118}, twice C_{70} gives C_{138}, and C_{60} plus C_{70} gives C_{128}. Accompanying each main peak is a well developed series corresponding to a stream of losses; for example, twice C_{70} yields C_{138} to C_{120} in a sharply truncated distribution. When no carrier gas is present to confine the desorbed vapour, these processes are barely observable, and give a very asymmetric distribution (Fig. 3, upper panel).

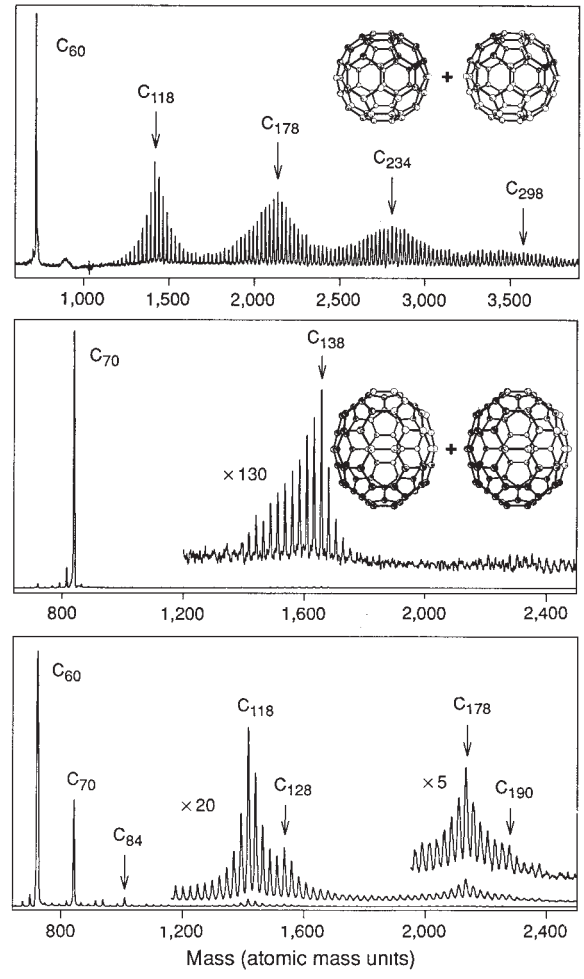

FIG. 2 Distributions generated as in Fig. 1, but for the specific fullerene materials and conditions as follows. *a*, Pure C_{60} sample, at higher laser fluence than that used in Fig. 1. *b*, Pure C_{70} sample, at very low fluence. The peak at C_{138} is also a ledge. The fragmentation extending downwards from C_{138} goes as far as C_{118} or even lower. *c*, Toluene extract of Krätschmer–Huffman soot, containing soluble fullerenes C_n, where $n=60$, 70, 76, 78, 82, 84, and trace amounts of higher fullerenes. Local maxima appear at $n=118$, 128, 178, 190, corresponding to combinations of nC_{60} and nC_{70}, $(n, m)=(2, 0)$, $(1, 1)$, $(3, 0)$, $(2, 1)$.

To verify that the reaction products are indeed strongly bound, rather than being simple aggregates held together by polarization forces or singly linking bonds, we collided the mass-selected C_{118}^+ beam with a solid surface (Si(111) terminated by hydrogen) at high velocity[19], and looked at the fragmentation pattern. As shown in Fig. 4, only a strongly scattered (intact) parent ion (C_{118}^+) and no fragments could be detected at energies of at least 200 eV. This result is similar to that obtained on other fullerenes[19–21]. Fullerene adducts, bound by pairs of external bonds, are readily broken at much lower energies (C.Y. and R.L.W., manuscript in preparation). A lower bound of ~6 eV on the energy of processes such as $C_{118} \rightarrow C_{60} + C_{58}$ is thereby estimated, using standard statistical rate theory arguments and energy-transfer assumptions documented elsewhere[19–22]. This value is inconsistent with a small number of bonds linking the cages, but is consistent with the integrity of known fullerene molecules. Furthermore, the shift in the time-of-flight indicates that these collisions are highly elastic up to an energy of 80 eV, and are increasingly inelastic thereafter.

Because coalescence products are strongly enhanced by the presence of a confining external gas (helium), it is clear that the processes are occuring in the dense vapour phase on a timescale of $\sim 10^{-5}$ s, rather than in the solid on a timescale of 10^{-7} s. This vapour is estimated to contain typically 10^{13} molecules in a volume of typically 10^{-3} cm^3, so that fullerene–fullerene collisions initially occur with very high frequency. The almost complete absence of smaller fragments such as C_{58} and C_{56} in all these distributions argues against a significant role for them in this process. The vapour temperature is not easily estimated, but the absence of C_{60} fragments, estimated to require 11 eV (ref. 16), gives an upper bound.

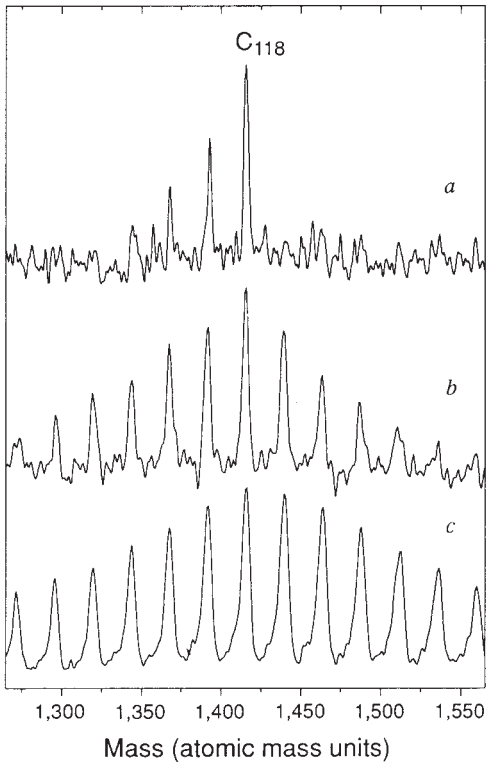

FIG. 3 Fluence dependence and effect of carrier gas on the coalescence product distribution obtained from C_{60}, shown in the region C_{106} to C_{130}. In *a*, no carrier gas was used, so there was no confinement of the desorbed vapour. In *b* and *c*, the carrier gas was present, but the fluence was reduced strongly in *b* from the conditions in Figs 1 and 2*a*. Decreasing the fluence or removing the helium carrier gas both cause a transition from a symmetric distribution around C_{118} (*c*), for higher vapour density, to a asymmetric one with a ledge at C_{118} (*b*, *a*) at lower vapour density. At the low-density conditions of *a*, the direct coalescence product C_{120} is completely absent, as are products of capture processes (C_{122} and higher).

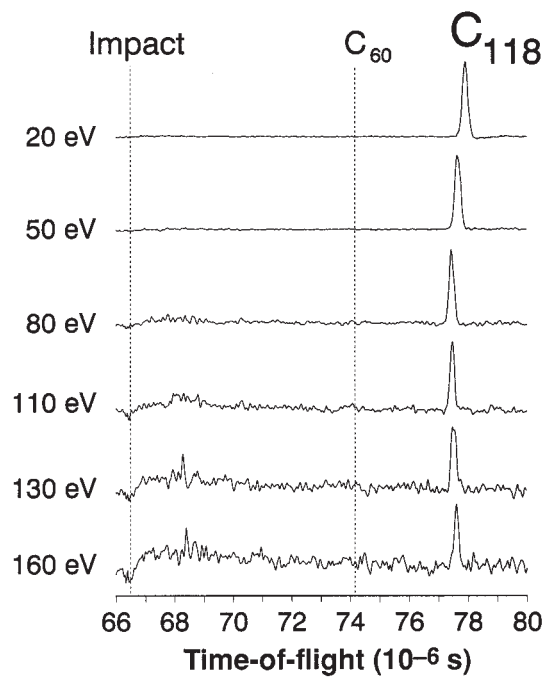

FIG. 4 Impact of C_{118}^+, mass-selected from a coalescence distribution, against a Si(111) surface. These time-of-flight mass spectra of scattered clusters show a complete absence of fragmentation, for example to C_{60} plus C_{58}, for energies to at least 160 eV. The approximate locations of the time of impact and the time where the C_{60} fragment would appear are marked. The time-shift of the scattered C_{118}^+ signal reflects the elasticity of the collision at low energy (shift to earlier time) and inelasticity at higher impact energy (shift toward later time). By comparison to known processes (such as $Na_{63}F_{62}$ with 125 atoms), we place a lower bound of 6 eV on the energy of breakup.

The asymmetric mass distributions around each coalescence maximum at the lower fluences indicate that coalescence processes are highly energetic and release excess energy through fragmentation processes, for example $C_n + C_m \rightarrow C_{n+m} \rightarrow C_{n+m-2} + C_2$. Fragmentation by emission of small even-numbered units is characteristic of hot giant fullerenes[23]. According to the calculations of Adams *et al.*[18], the rapid increase of the cohesive energy (with size) toward graphite implies an energy release per atom (total) of 0.16 eV (19 eV) for $2\ C_{60} \rightarrow C_{120}$, 0.24 eV (43 eV) to produce C_{180}, and 0.28 eV per atom (67 eV) to produce C_{240}. In the hot vapour, this entire energy might be released through emision of two or more small (C_2) or larger (C_4 or C_6) even-numbered fragments. The statistical nature of the cooling is expressed by a large range of fragments, peaking at a single C_2 loss but extending all the way to 16 C loss (for C_{60} dimerization) or 22 C loss (for C_{70} dimerization).

A second effect, appearing as a mass gain that makes the distributions symmetrical under higher-density conditions (Figs 1 and 2*a*), requires that these small emission fragments are captured by previously coalesced fullerenes in the dense vapour to produce heavier species, for example $C_{118} + C_4 \rightarrow C_{122}$. Recalling that the vapour density is very high at the higher fluences, it is natural to propose that the small fragments generated through evaporative cooling do not escape the hot zone, as they would in low-density vapours, but instead collide and react with other fullerenes, including the nascent coalescence products. It may be significant that these capture processes do not occur for C_{60} to C_{70} (note the absence of C_{62}, C_{64} or C_{72}), a fact which may be related to their postulated reluctance to grow in contact with carbon vapour[25]. The combined evaporation-and-capture reaction process can be regarded as an exchange mechanism

that broadens (more or less symmetrically) the abundance distributions. A detailed mathematical analysis of these distributions, within a kinetic model of coalescence and capture processes, will be presented elsewhere (K.H., manuscript in preparation). An alternative hypothesis for forming species such as C_{122}, involving fullerenes such as C_{62} and C_{64}, is untenable, as they are not present in the vapour.

The experiments described here are of limited use in determining the precise kinetics of coalescence at known temperatures; a precision measurement of the reaction yield requires collecting and weighing the higher fullerene material generated. Experiments towards these goals are in progress. One concern is the role of charge, as we have not detected coalescence products in the negative-ion channel. It is possible that coalescence is accelerated in a plasma environment. (For example, if the initial temperature were 2,500 K, and given the known difference of ~4.8 eV between ionization potential and electron affinity for either C_{60} or C_{70}, then the fraction of charged pairs is 10^{-8}, or a total of 10^5 pairs per pulse, in our case.) Further information on the reaction dynamics could be provided by a study of nonthermal processes. Campbell *et al.*[24] have collided an accelerated beam (850 eV) of C_{60}^+ ions with thermal C_{60} molecules and found that heavier ions (not mass-resolved, but covering the C_{90}–C_{120} range) are generated.

The existence of efficient coalescence reactions has implications for fullerene research and applications, most obviously concerning the long-time stability of fullerene vapours and plasmas, and for the growth and formation processes, where coalescence must be resisted so as to stabilize C_{60} and C_{70} in high yield. Controlled coalescence might be used to produce large quantities of selected higher fullerenes such as C_{120}, C_{130} and C_{140}, where higher inert gas pressure is required to remove the heat of coalescence. We have begun to investigate this possibility. Coalescence processes may also be involved in the formation of larger encapsulation compounds which can involve the fusion of empty fullerenes in the presence of metal[26–28]. A related process may be involved in the degradation of pure fullerene solids. For example, Wang and Buseck[29] have reported that electron-beam irradiation in an electron microscope stimulates growth of larger structures that may be fullerenes. □

Received 19 June; accepted 5 August 1992.

1. Krätschmer, W., Lamb, L. D., Fostiropoulos, K. & Huffman, D. R. *Nature* **347,** 354 (1990).
2. Peters, G. & Jansen, M. *Angew. Chem. Int. Ed. Engl.* **31,** 223 (1992).
3. Howard, J. B., McKinnon, J. T., Makarovsky, Y., Lafleur, A. & Johnson, M. E. *Nature* **352,** 139–141 (1991).
4. Ajie, H. *et al. J. phys. Chem.* **94,** 8630–8633 (1990).
5. Taylor, R., Hare, J. P., Abdul-Sada, A. K., Kroto, H. W. *J. chem. Soc. Chem. Commun.* 1423–1425 (1990).
6. Allemand, P.-M. *et al. J. Am. chem. Soc.* **112,** 1050–1051 (1990).
7. Haddon, R. C. *et al. Nature* **350,** 320–323 (1991).
8. Suzuki, T., Li, Q., Khemani, K. C., Wudl, F. & Almarsson, Ö. *Science* **254,** 1186–1187 (1991).
9. Krusic, P. J., Wasserman, E., Keizer, P. N., Morton, J. R. & Preston, K. F. *Science* **254,** 1183–1185 (1991).
10. Chai, Y. *et al. J. phys. Chem.* **95,** 7564–7568 (1991).
11. Weiske, T., Böhme, D. K., Hrusak, J., Krätschmer, W. & Schwarz, H. *Angew. Chem. int. Ed. Engl.* **30,** 884–886 (1991).
12. Ross, M. M. & Callahan, J. H. *J. phys. Chem.* **95,** 5720–5723 (1991).
13. Kroto, H. W. *Angew. Chem. int. Ed. Engl.* **31,** 111–129 (1992).
14. Diederich, F. & Whetten, R. L. *Acct. chem. Res.* **25,** 119–126 (1992).
15. Beckhaus, H.-D., Rüchardt, C., Kao, M., Diederich, F. & Foote, C. S. *Angew. Chem. int. Ed. Engl.* **31,** 63–64 (1992).
16. Stanton, R. E. *J. phys. Chem.* **96,** 111–118 (1992).
17. Zhang, B. L., Wang, C. A., Ho, K. M. *Chem. Phys. Lett.* **193,** 225–230 (1992).
18. Adams, G. B., Sankey, O. F., Page, J. B., O'Keeffe, M. & Drabold, D. A. *Science* **256,** 1792–1795 (1992).
19. Beck, R. D., St. John, P., Alvarez, M. M., Diederich, F. & Whetten, R. L. *J. phys. Chem.* **95,** 8402–8409 (1991).
20. Busmann, H.-G., Lill, Th. & Hertel, I. V. *Chem. Phys. Lett.* **187,** 459–465 (1990).
21. Busmann, H.-G., Lill, Th., Reif, B. & Hertel, I. V. *Surf. Sci.* **272,** 146–153 (1992).
22. Yeretzian, C. & Whetten, R. L. *Z. Phys. D* (in the press).
23. Maruyama, S., Lee, M. Y., Haufler, R. E., Chai, Y. & Smalley, R. E. *Z. Phys. D,* **19,** 409 (1991).
24. Campbell, E. E. B., Hielscher, A., Ehlich, R., Schyja, V. & Hertel, I. V. in *Nuclear Physics Concepts in the Study of Atomic Cluster Physics* (eds Schmidt, R., Lutz, H. O. & Dreizler, R.) Lecture Notes in Physics Vol. 404, 185 (Springer, 1992).
25. Kroto, H. W., Heath, J. R., O'Brien, S. C., Curl, R. F., Smalley, R. E. *Nature* **318,** 162–163 (1985).
26. McElvany, S. W., Ross, M. M. & Callahan, J. H. *Acct. chem. Res.* **25,** 162–168 (1992).
27. Jin, C., Guo, T., Chai, Y., Lee, A. & Smalley, R. E. *Fullerene Nanowires, Proc. 1st Italian Workshop on Fullerenes, 6–7 February 1992* (eds Taliani, C., Ruani, G. & Zamboni, R.) (World Scientific, 1992).
28. Smalley, R. E. in *Naval Res. Rev.* **3,** 3–14 (1991).
29. Wang, S. & Buseck, P. R. *Chem. Phys. Lett.* **182,** 1–4 (1991).

ACKNOWLEDGEMENTS. We acknowledge L. Issacs for supplying pure C_{60} and C_{70}, and M. M. Alvarez and R. D. Beck for their roles in early experiments leading to this research. This research has been supported by the NSF, an ONR contract, a postdoctoral fellowship to C.Y. from the Schweizerischer Nationalfonds, a grant to K.H. from the Nørgård Foundation and a Packard Foundation Fellowship to R.L.W.

Enhancements in biologically effective ultraviolet radiation following volcanic eruptions

A. M. Vogelmann, T. P. Ackerman & R. P. Turco*

Department of Meteorology, The Pennsylvania State University, University Park, Pennsylvania 16802, USA
* Department of Atmospheric Sciences, University of California, Los Angeles, California 90024, USA

AEROSOLS injected into the stratosphere by large volcanic eruptions may induce ozone destruction through processes including heterogeneous chemical reactions. The effect of ozone reductions on surface ultraviolet irradiation is not obvious, however, because aerosols also increase the reflection of sunlight. Here we use a radiative transfer model to estimate the changes in biologically effective ultraviolet radiation (UV–BE) at the Earth's surface produced by the El Chichón (1982) and Mount Pinatubo (1991) eruptions. We find that in both cases surface UV–BE intensity can increase because the effect of ozone depletion outweighs the increased scattering.

Ozone is the primary absorber of the Sun's ultraviolet radiation, which is potentially harmful to plants and animals. It is possible that short-term ozone depletions are caused by large volcanic eruptions, which inject millions of tons (Mt) of SO_2 into the stratosphere where it then forms an H_2SO_4 (sulphuric acid) aerosol. This aerosol provides surfaces on which heterogeneous chemical reactions are able to activate chlorine into forms that catalyse ozone destruction[1,2]. The potential for ozone destruction increases with volcanic aerosol loading and with stratospheric chlorine concentrations. (The primary source of stratospheric chlorine is anthropogenic, as the amount of chlorine injected into the stratosphere by volcanos seems to be small[3].) If the sulphate aerosol loading were to reach certain critical values, it is possible that catastrophic ozone loss rates could occur[4], similar to those in the Antarctic spring. Further, the aerosol alters the stratospheric radiative and temperature fields, so it may affect photodissociation rate constants so as to decrease ozone concentrations[5]. Although theory suggests that ozone depletions may result from volcanic eruptions, observational evidence for this is uncertain.

El Chichón erupted in March and April of 1982, causing chemical and radiative perturbations on a global scale[6]. Ozone column depletions of 1–7% were observed in many regions of the world, with even larger depletions observed at specific monitoring stations[7–10]. The ozone depletions typically started in late autumn, peaked in winter, and returned to normal levels by summer. During the December–April period after the eruption, some Northern Hemisphere stations reported the lowest monthly values measured in 40 years[7,8]. The relationship between these ozone depletions and the volcanic eruption is obscured by other phenomena occurring at that time, such as the westerly phase of the quasibiennial oscillation (QBO), or the abnormally intense El Niño/Southern Oscillation (ENSO)[7,8]; analyses indicate, however, that the aerosol was reponsible for a depletion of 2–10% in the affected layers[1,8,10].

Mount Pinatubo erupted in June of 1991, injecting almost